The Optical Properties of a Truncated Spherical Cavity Embedded in Gold

Anders Pors[*1], Ole Albrektsen[2], Sergey I. Bozhevolnyi[2], and Morten Willatzen[1]
[1]Mads Clausen Institute, University of Southern Denmark, Sønderborg
[2]Institute of Sensors, Signals and Electrotechnics, University of Southern Denmark, Odense
*Corresponding author: pors@mci.sdu.dk

Abstract: The use of plasmonic effects to dramatically enhance the electromagnetic field near the surface of a metallic nanostructured surface has grown into a large research area in the effort to take advantage of the surface enhanced field.
In this paper the electromagnetic field near a nano-sized truncated spherical cavity embedded in a gold substrate is investigated and modeled in 3D with COMSOL Multiphysics. An essential computational problem here is to setup a model that is independent of the width of the simulation domain.
The simulated near-field is interpreted on the basis of Mie-theory and resonance of localized surface plasmon polaritons (LSP).
The optical properties, such as absorption and scattering of light, of the truncated spherical cavity are also investigated. It is found that LSP resonances mainly affect the scattering, which is due to the spatial shape of the LSPs. It is at the same time possible to control the scattering property by changing the size of the cavity.

Keywords: Plasmon, Mie-theory, spherical cavity, electromagnetic field.

1. Introduction

The interest in the electromagnetic field close to metallic nanostructures has increased in the last decades due to the possibility of fabricating, characterizing, and utilizing nanostructures. In metallic nanostructures the electromagnetic field (EM-field) may excite collective vibrations of the conduction-band electrons - also known as plasmons. The EM-field and the plasmons interact with each other, and the coupled state is called a surface plasmon polariton (SPP) which properties depend on the geometry and size of the nanostructure. When the spatial extension of the plasmon excitation is small compared to the wavelength of the light, the coupled state is called a localized surface plasmon polariton (LSP) [1]. LSP has the ability to dramatically enhance the EM-field in the vicinity of the nanostructure which can be utilized to increase the sensitivity in a variety of different sensor applications. One of the most interesting applications is surface-enhanced Raman spectroscopy where single-molecule detection is possible.

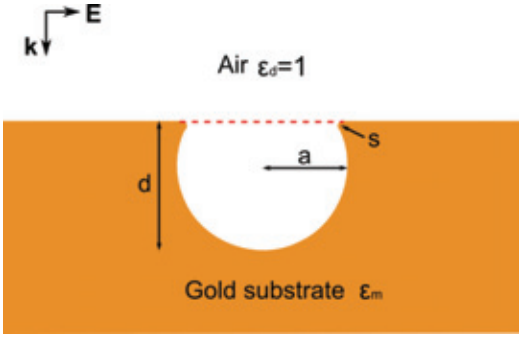

Figure 1. Cross-section of a truncated spherical cavity embedded in gold with dielectric constant ε_m. The cavity has radius *a*, depth *d* and the rim is rounded with a radius *s*. The red dashed line indicates the aperture for far-field calculation.

A nanostructure, which is relatively easily fabricated, is a truncated spherical cavity embedded in gold [2]. A schematic cross-section of the structure is shown in figure 1. In this paper, the EM-field in the vicinity of a truncated spherical cavity embedded in gold is investigated through 3D finite element simulations with COMSOL Multiphysics. The paper also includes an investigation of the ability of the cavity to scatter and absorb light when the incoming light is a plane wave propagating perpendicular to the gold surface. The simulations are interpreted on the basis of Mie-theory.

2. The Truncated Spherical Cavity

The electromagnetic field in a spherical cavity embedded in an infinite metallic substrate is analytically described with the Mie-theory. When the incoming field is a plane wave, the field inside the cavity $\mathbf{E}_{in}$ is given by [3]

$$\boldsymbol{E}_{in} = \sum_{n=1}^{\infty} E_n (c_n \boldsymbol{M}_{1n} - i d_n \boldsymbol{N}_{1n}), \qquad (1)$$

where $E_n c_n$ and $E_n d_n$ are the amplitudes, c_n and d_n expansion coefficients, and $\boldsymbol{M}_{1n}$ and $\boldsymbol{N}_{1n}$ are known as spherical vector harmonics (SVH) that are characterized by two integers m and n where m=1. The internal field is in general a superposition of SVH. However, at certain wavelengths an expansion coefficient can be in resonance and the corresponding SVH will dominate. Physically, the resonance corresponds to an excitation of a LSP.

Even though the spherical cavity is well described, it is of no experimental interest, because the incoming light will never be able to excite LSPs in the cavity due to the (infinite) thick metallic substrate. A much more interesting structure is the truncated spherical cavity that is embedded in metal with the opening pointing into a half-space of air (fig. 1). Unfortunately, there is no analytical solution to this geometry. However, the results from the spherical cavity can be used as a starting point in describing the optical/plasmonic properties of a truncated spherical cavity, as explained in [4]. The LSPs of a truncated spherical cavity are a result of coupling between Mie-modes (spherical cavity) and rim-LSPs resulting in low-energy bonding states $\boldsymbol{M}_{1n}^{+}$ and $\boldsymbol{N}_{1n}^{+}$ and high-energy anti-bonding states $\boldsymbol{M}_{1n}^{-}$ and $\boldsymbol{N}_{1n}^{-}$. The principle of the LSP-coupling is shown in figure 2.

It should be mentioned that the integer m might take on other values than 1 when the incoming field is not perpendicular to the surface of the substrate [4]. However, in this paper we limit ourselves to perpendicular incoming waves.

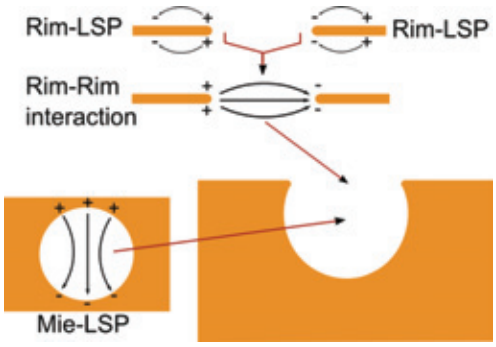

Figure 2. A sketch of the coupling between the different LSP-components in a truncated spherical cavity.

3. The Basic Equations

Even though the interaction between the EM-field and the conduction electrons in the metal is a quantum mechanical phenomenon, the huge numbers of electrons in the metal makes the interaction suited for a classical description with Maxwell's equations. In the following it is assumed that no currents and excess charges exist in the simulation domain, where the E- and H-fields oscillates harmonically in time. The electric (or magnetic) field can be computed by solving the vector wave equation:

$$\nabla \times \left(\frac{1}{\mu} \nabla \times \boldsymbol{E} \right) - k_0^2 \varepsilon \boldsymbol{E} = 0, \qquad (2)$$

In the equation $\boldsymbol{E}$ is the electric field, k_0 is the wave number in free space, and ε and μ are the relative permittivity (dielectric constant) and relative permeability, respectively.

The optical properties of a geometry is characterized by its ability to absorb and scatter light. If the material is a metal (lossy medium) some of the electromagnetic energy is converted to heat. The amount of averaged dissipated energy U_{abs} is given by [5]

$$U_{abs} = -\frac{1}{2} \omega \, \mathrm{Im}[\varepsilon_m] |\boldsymbol{E}|^2, \qquad (3)$$

where ω is the angular frequency, and ε_m the dielectric function of the metal. In the above formula, time-averaging is performed on time-harmonic fields.

It is a much more problematic task to calculate the scattered light of the geometry in figure 1, because it is necessary to calculate the far-field (radiation field) from the knowledge of the field near the geometry. One way of calculating the far-field is by use of the Stratton-Chu formula [6] and the far-field approximations for the free-space Green function and the ∇-operator [7]:

$$\boldsymbol{E}_{far}(\boldsymbol{r}) = \frac{-ike^{-ikr}}{4\pi r} \hat{\boldsymbol{r}} \times \int_S \left[(\hat{\boldsymbol{n}} \times \boldsymbol{E}_s) - \eta (\hat{\boldsymbol{r}} \times (\hat{\boldsymbol{n}} \times \boldsymbol{H}_s)) \right] e^{ik\hat{\boldsymbol{r}} \cdot \boldsymbol{r}'} dS' \qquad (4)$$

In the above formula, $\boldsymbol{r}$ is the position in the far-field where we want to calculate the E-field, r=|**r**|, k is the wave number, $\hat{\boldsymbol{r}}$ is the unit vector pointing in direction of $\boldsymbol{r}$, $\hat{\boldsymbol{n}}$ is the outward normal-vector to the surface S, η is the vacuum

impedance. The formula tells us that the far-field may be computed from the knowledge of the scattered E- and H-field ($\boldsymbol{E}_s$ and $\boldsymbol{H}_s$) on the surface *S*, where the scattered field is defined as the part of the total field which radial component asymptotically behaves as a spherical wave.
For the geometry in figure 1, the surface *S* must be the infinite plane surface separating the half-space of gold (including the cavity) with the half-space of air. Unfortunately it is not practically possible to simulate an infinite wide gold substrate, so the surface *S* is limited to the aperture of the cavity (indicated by a red dashed line in figure 1). This approximation is known as Kirchhoffs' Second Approximation.
When the far-field is calculated, it is possible to calculate the average intensity scattered into the far-field:

$$U_{sca} = \frac{1}{2\eta}\left|\boldsymbol{E}_{far}\right|^2 \qquad (5)$$

It should be noticed that the above formula is only valid in the far-field where the E- and H-fields are perpendicular to each other.

4. The COMSOL model

Even though the geometry of a truncated spherical cavity embedded in gold has cylindrical symmetry, it is still necessary to do 3D simulations when we use a linearly polarized light as the incoming wave. The total system (geometry + perpendicular incoming wave) does, however, contain two symmetry planes, so only one quarter of the full geometry needs to be modeled. On the other hand, it is necessary to do the simulation in 2 steps so that the final solution is independent of the width of the simulation domain. The 2-step procedure is shown in figure 3 and will be explained in the following.

In step 1, eq. (2) is solved for the reflection and refraction of a perpendicular incoming wave by a plane gold substrate (no cavity). The simulation uses the application *harmonic propagation* in the RF-module. The vertical boundaries (boundary 1, 2, 4, 5) are pairwise either perfect electric conductor (PEC) or perfect magnetic conductor (PMC) which forces the incoming wave to be perpendicular to the boundaries. The plane wave behaves as if the width of the gold substrate is infinite (independent of the width of the simulation domain).

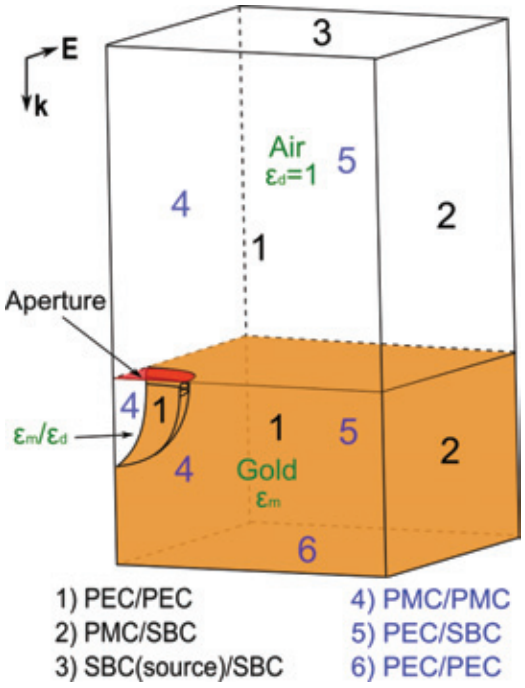

Figure 3. The COMSOL model. The numbers indicate the type of boundary condition, where the blue numbers belongs to the boundaries hidden in the figure if the model wasn't transparent. The boundary conditions may change between the two simulations, where e.g. "PMC/SBC" should be understood as: In step 1 the boundary is PMC, while it is an open boundary with SBC in step 2. Green text indicates subdomain specifications.

In step 2, eq. (2) is solved with the COMSOL application *scattered harmonic propagation*, where the E-field from the simulation in step 1 is used as the incoming field. However, this time the gold substrate contains a truncated spherical cavity, and the vertical boundaries, while not being symmetry planes, behave as open boundaries using the *scattering boundary condition* (SBC). According to the *scattered field formulation* [8], sources will only be generated in the cavity and not in the gold substrate due to the choice of the incoming field. The result is a simulation of the EM-field near the cavity with the opening pointing into an open region of air that is independent of the width of the simulation domain.

In the simulations the dielectric function of the gold substrate ε_m is described by an interpolated version of the often used experimental data from Johnson and Christy [9].

4.1 The Effective Cross Section

A quantity that is related to experimental observations is the effective cross section of a geometry which is a measure of the cross section in relation to the geometrical cross section. The effective absorption cross section Q_{abs} is related to the dissipated energy due to the cavity and is defined as:

$$Q_{abs} = \frac{4}{\pi a^2}\frac{2\eta}{E_0^2}\int_{V_{cav}} U_{abs2} - U_{abs1} dV \,. \quad (6)$$

In the formula πa^2 is the geometrical cross section of the cavity, the normalization factor $\frac{1}{2\eta}E_0^2$ is the average intensity of the incoming plane wave, the number 4 is to account for only simulating on quarter of the geometry, and U_{abs1} and U_{abs2} are the dissipated energy after step 1 and 2, respectively. The integration volume V_{cav} corresponds to the 100nm gold surrounding the cavity. By integrating U_{abs1}-U_{abs2} the resulting cross section is only due to the presence of the cavity and not the regular dissipation of energy in the plane gold substrate.

The effective scattering cross section Q_{sca} is calculated from the electric far-field:

$$Q_{sca} = \frac{4}{\pi a^2}\frac{2\eta}{E_0^2}\frac{1}{R_{\text{int}}^2}\int_{S_{sph}} U_{sca} R_{\text{int}}^2 dS \,. \quad (7)$$

The integration is performed over one quarter of a sphere with radius R_{int} and area S_{sph}. COMSOL automatically normalizes the integrand with R_{int}^2, so in eq. (7) it is necessary to divide by the same factor [10]. It should be mentioned that the electric far-field is calculated from the scattered field in step 2 with the built-in far-field post-processing tool using the aperture indicated in figure 3.

5. Results of modeling

5.1 Excitation of LSP modes

By the knowledge of the spatial distribution of the different SVH (Mie-mode), it is advantageous to track how the E-field changes in certain strategic positions (positions where the SVHs have maxima and minima) in the truncated cavity when the wavelength of the incoming wave changes. A distinct minimum or maximum in the E-field is generally an indicator of resonance of a certain coupled LSP mode.

By the procedure just described above, figure 4 presents a selection of the detected lowest ordered LSP modes for a cavity with parameters a=500nm, d=900nm and s=10nm. Figure 4a,b are the bonding and anti-bonding state of the Mie-mode $\mathbf{N}_{11}$ while figure 4c,d are the coupled states of $\mathbf{N}_{12}$. It is evident that the anti-bonding states (figure 4b,d) more closely resembles the pure Mie-modes, while the bonding states (figure 4a,c) are strongly perturbed by the rim and the coupling to the rim-mode. The bonding states are characterized by having the largest field enhancement at the rim, while the anti-bonding states have the enhancement in the cavity. The field enhancement is generally larger for the bonding states, which probably is not only due to plasmonic effects, but also the electrostatic *lightning rod effect* [11] at the rim.

5.2 Absorption and scattering

The effective absorption and scattering cross sections are calculated for cavities of different sizes, but with the truncation parameter d/(2a) equal to 0.8 at all times. The result is shown in figure 5. The absorption cross section (figure 5a) has no distinct maxima and minima, but rather a broad band of absorption for wavelengths below 550nm. It is only possible to identify a weak increase in absorption for the $\boldsymbol{N}_{11}^{+}$ and a minima in absorption for $\boldsymbol{N}_{11}^{-}$. The difference is due to the spatial shape of the modes. However, in general, figure 5a illustrates that the absorption is only weakly dependent on excitation of LSPs. The reason is again the spatial profile of the modes in figure 4, where the field-enhancement takes place in the air and near the surface of the substrate, but no significant enhancement is observed in the gold and therefore no increase in absorption. This is also why Q_{abs} decreases for larger cavities, because Q_{abs} is divided by a larger cross section πa^2 without a corresponding increase in absorption. The wide band of absorption below 550 nm is related to the optical properties of gold (plasma frequency) and not the nanostructured surface. An almost equivalent absorption profile will be present for a plane gold substrate.

The behavior of the scattering cross section is very much different compared to the absorption cross section. The spectrum contains some distinct minima and maxima that can be related to the excitation of specific LSPs (some of them

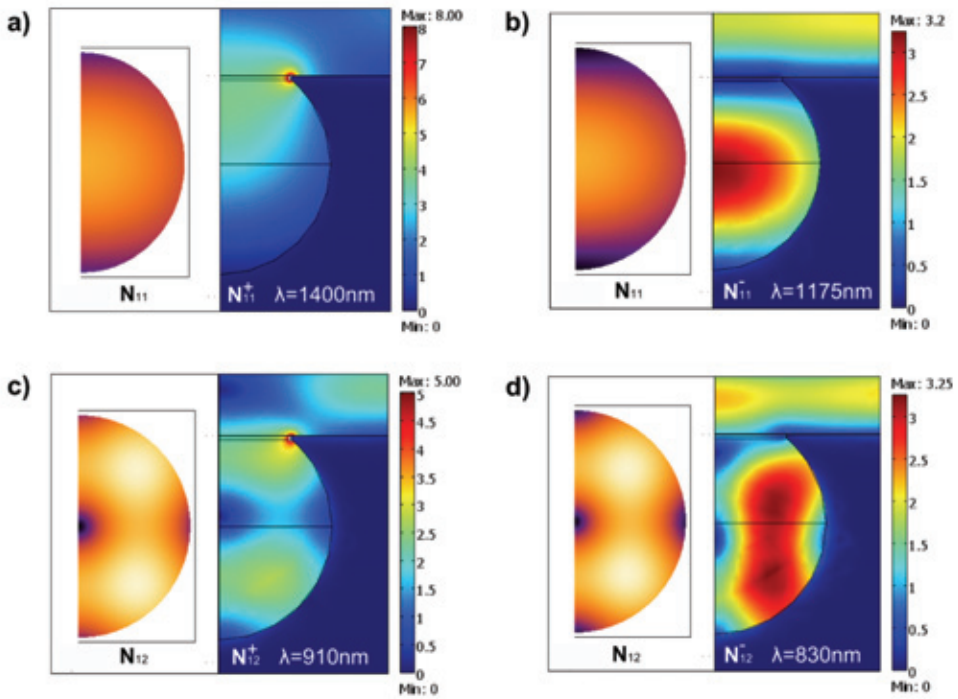

Figure 4. A selection of LSP modes in the truncated cavity embedded in gold with parameters a=500nm, d=900nm, s=10nm. Left side in each figure shows the unperturbed Mie-mode (bright areas correspond to high intensity), while the right side shows the simulation result of the absolute value of the E-field in [V/m] in a cross section through the cavity at a certain wavelength λ, when the incoming wave has the amplitude E_0=1V/m. The white spots in figure a) and c) are areas where the E-field is higher than the scale on the color bar.

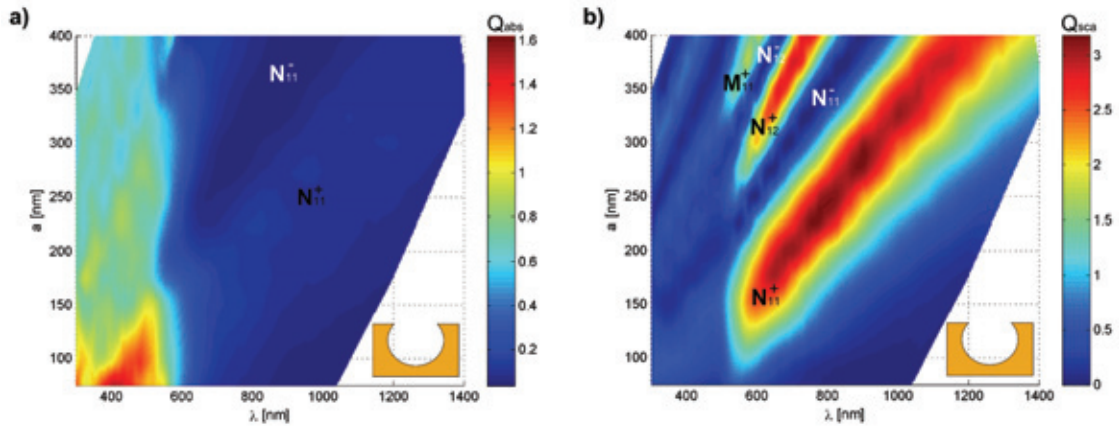

Figure 5. a) Effective absorption cross section Q_{abs} for a truncated spherical cavity with the truncation parameter d/(2a)=0.8 as a function of the wavelength of the incoming field λ and the radius of the cavity *a*. b) The effective scattering cross section Q_{sca}.

shown in figure 4). However, calculations show that only the bonding states give rise to an increased scattering whereas anti-bonding states are seen as minima in the figure. This behavior must be due to the spatial shape of the modes, where bonding states have the significant field-enhancement at the rim of the cavity thus behaving as sources of scattering.

Figure 5b shows that for cavities with radius a<250nm it is only possible to excite the

fundamental broad mode $\boldsymbol{N}_{11}^{+}$. However, when the radius of the cavity increases it might be possible to excite higher order modes such as $\boldsymbol{N}_{12}^{+}$. A behavior like this is typical for nanostructured systems.
Another interesting result in figure 5b is the possibility to partly control the optical response of the cavity by changing the radius. The spectral position of the LSP-modes red-shifts (almost linearly) when the radius of the cavity increases making the geometry a possible candidate as a tunable substrate for surface enhanced sensing. The insensitivity of the spectral position of $\boldsymbol{N}_{11}^{+}$ for cavities with a<150nm is a consequence of the quasi-static regime where retardation effects have a weak influence on the behavior of the plasmons and the resonance conditions [12].

We may conclude that the optical properties of a truncated spherical cavity embedded in gold are characterized by the scattering and not the absorption. A similar conclusion is made in ref. [2] based on reflection measurements on gold substrates containing spherical voids.

6. Conclusion

In this paper the electromagnetic near-field and the optical properties of a truncated spherical cavity embedded in gold is investigated with a 3D model implemented in COMSOL Multiphysics. The model uses a 2-step simulation procedure that makes the simulation result independent of the width of the simulation domain.

The simulated near-field is interpreted on the basis of Mie-theory. It is evident that at certain wavelengths of the incoming wave, LSPs will be excited generating a characteristic near-field (mode shape) in and near the opening of the cavity.
The effective absorption and scattering cross sections are calculated from the simulated results. It is clear that only the scattering is significantly affected by excitation of LSPs, which is due to the spatial shape of the modes. Excitation of bonding states increases the scattering whereas the opposite is true for anti-bonding states. Simulations also show the possibility to modify the scattering property (resonance of LSP) by changing the size of the cavity.

7. References

1. S. A. Maier, Plasmonics: Fundamentals and Applications, pp. 65-88, Springer (2007).
2. P. N. Bartlett et al., Optical Properties of Nanostructured Metal Films, Faraday Discuss., **125**, 117-132 (2004).
3. C. F. Bohren, D. R. Huffman, Absorption and Scattering of Light by Small Particles, pp. 93-94, Wiley (1983).
4. R. M. Cole et al., Understanding Plasmons in Nanoscale Voids, Nano Lett., **7**, 2094-2100 (2007).
5. J. D. Jackson, Classical Electrodynamics, 3. edition, pp. 262-264, Wiley (1999).
6. J. A. Stratton, L. J. Chu, Diffraction Theory of Electromagnetic Waves, Phys. Rev., **56**, 99-107 (1939).
7. J. D. Jackson, Classical Electrodynamics, 3. edition, pp. 482-485, Wiley (1999).
8. J. Jin, The Finite Element Method in Electromagnetics, 2. edition, pp. 553-554, Wiley (2002).
9. P. B. Johnson et al., Optical Constants of the Noble Metals, Phys. Rev. B, **6**, 4370-4379 (1972.)
10. M. W. Knight et al., Nanoshells to Nanoeggs to Nanocups: Optical Properties of reduced Symmetry Core-Shell Nanoparticles beyond the Quasistatic Limit, New J. Phys., **10**, 105006 (2008).
11. P. M. Fishbane et al., Physics for Scientists and Engineers with Modern Physics, 3. Edition, pp. 700-702, Pearson Prentice Hall (2005).
12. M. Pelton et al., Metal-Nanoparticle Plasmonics, Laser & Photon. Rev., **2**, 136-159 (2008).